A non-coaxial critical-state model for sand accounting for fabric anisotropy and fabric evolution

Zhiwei Gao[1*], Jidong Zhao[2]

[1] School of Engineering, Rankine Building, University of Glasgow, Glasgow, G12 8LT, UK

[2] Department of Civil and Environmental Engineering, Hong Kong University of Science and Technology, Hong Kong SAR, China

[*] Corresponding author. Email: Zhiwei.gao@glasgow.ac.uk. Tel: +44 (0)141 330 3927

Abstract: Soil fabric and its evolving nature underpin the non-coaxial, anisotropic mechanical behaviour of sand, which has not been adequately recognized by past studies on constitutive modelling. A novel three-dimensional constitutive model is proposed to describe the non-coaxial behaviour of sand within the framework of anisotropic critical state theory. The model features a plastic potential explicitly expressed in terms of a fabric tensor reflecting the anisotropy of soil structure and an evolution law for it. Under monotonic loading, the fabric evolution law characterizes a general trend of the fabric change to gradually become co-directional with the loading direction before the soil reaches the critical state. When a sand is subjected to rotation of principal stress directions, the fabric evolves with the plastic strain increment which is further dependent on the current stress state, the current fabric and the direction of stress increment. During its evolution, the fabric rotates towards the loading direction and reaches a final degree of anisotropy proportional to a normalized stress ratio. With the incorporation of fabric and fabric evolution, the non-coaxial sand behaviour can be easily captured, and the model response converges to be coaxial at the critical state when the stress and fabric are co-directional. The model has been used to simulate the mechanical behaviour of sand subjected to either monotonic loading or continuous rotation of principal stress directions. The model predictions agree well with test data.

Keywords: Sand; anisotropy; constitutive model; fabric evolution; noncoaxiality; rotation of principal stress directions

1. INTRODUCTION

Non-coaxial sand response refers to an inconsistency of the principal axes of plastic strain increment and those for the stress. It is commonly observed in experimental tests on both naturally deposited and reconstituted sands (Roscoe, 1970; Li and Yu, 2010; Rodriguez and Lade, 2014). Roscoe (1970) is among the first to observe the non-coaxial behaviour in his simple shear tests on sand. His tests show that the principal strain rate and the principal stress are more non-coaxial at lower shear strain level. They tend to be more coaxial when the shear strain increases, and become totally coaxial when the sand reaches the critical state. Similar non-coaxial response has also been observed in hollow cylinder torsional shear tests with fixed principal stress directions and variable intermediate principal stress (Symes et al., 1984; Gutierrez et al., 1991; Miura et al., 1986; Rodriguez and Lade, 2014). Rather apparent non-coaxial response has been observed in sand subjected to continuous rotation of principal stress axes (Gutierrez et al., 1991; Miura et al., 1986; Nakata et al., 1998; Yang et al., 2007). These tests indicate that the degree of non-coaxiality, defined by the relative angle between the principal plastic strain increment direction and that of the stress, depends on both the stress ratio and fabric anisotropy. For example, higher degree of non-coaxiality is observed in more anisotropic samples at relatively lower stress ratio, and it gradually diminishes as the stress ratio approaches the critical state.

Proper understanding of the non-coaxial behaviour of sand can be of great theoretical significance and practical importance. For example, when an offshore geo-structure is subjected to wave loads or a embankment pavement is subjected to repeated traffic loads, it may lead to continuous rotation of principal stress directions and induce significant accumulation of non-coaxial plastic deformation in relevant soils over a sustained period of loading, which may potentially cause liquefaction to the offshore geostructures or permanent distress to the road embankments (Ishihara, 1983). More recent micromechanical studies suggest that non-coaxial deformation may act as a crucial trigger for strain localization in anisotropic sand (Gao and Zhao, 2013; Guo and Zhao, 2014; Zhao and Guo, 2015), a phenomenon widely considered a key precursor for catastrophic failures such as landslide and debris flow. Due to its apparent importance, non-coaxial sand behaviour has been one of the focal topics in constitutive modelling of sand over the past two decades (e.g., Tobita and Yanagisawa, 1992; Gutierrez et al., 1993; Li and Dafalias, 2004; Qian et al., 2008).

A typical approach followed by most existing models in classic soil mechanics has been to simply assume that the plastic strain increment direction is dependent on both the current stress state and stress increment direction (Darve, 1974; Dafalias, 1975; Dafalias 1977; Dafalias, 1986; Gutierrez et al., 1993; Papamichos and Vardoulakis, 1995; Hashiguchi and Tsutsumi, 2003; Li and Dafalias, 2004; Yu and Yuan, 2006; Nicot and Darve, 2007; Lashikari and Latifi, 2008; Qian et al., 2008). This approach is coined by Dafalias (1986) as hypoplasticity which offers a viable pathway to capture the non-coaxial sand behaviour to a reasonable extent. However, it may not provide adequate links of the non-coaxial response in sand with the underpinning physical attributes and fundamental mechanisms. Rather clearer than ever, non-coaxiality is indeed a natural response exhibit by any anisotropic materials including sand. The crucial role played by fabric anisotropy in dictating the non-coaxial behaviour in anisotropic sand should be adequately recognized and explicitly considered. More importantly, the fabric exhibits an evolving nature with deformation, which serves as a crucial physical mechanism accounting for the change of non-coaxial response in sand (Li, 2013; Gao et al., 2014; Thornton and Zhang, 2006; Li and Yu, 2009; Li and Yu, 2010; Yang, 2013a; Guo and Zhao, 2014; Zhao and Guo, 2015; Oda and Konishi, 1974). As shown by the micromechanical studies of Li and Yu (2010), the fabric of granular materials will evolve (including changing in principal directions and magnitude) when they are subjected to shear. The rotation of fabric produces strain components normal to the stress direction, which accounts for non-coaxial sand response in rotation of principal stress directions. Evidently, fabric and fabric evolution are indispensable for modelling the non-coaxial sand behaviour (Yu, 2008). Proper consideration of fabric and its evolution in a model may help to simulate the non-coaxial behaviour in sand more rigorously. Indeed, there has been a number of non-coaxial sand models developed to account for the effect of inherent anisotropy, but without considering fabric evolution. For instance, Tobita and Yanagisawa (1992) have proposed using a yield function expressed in terms of a modified stress tensor dependent on both the stress tensor and fabric tensor. An associated flow rule based on this yield function has been used. The model can predict coaxial responses for an initially isotropic material and non-coaxial responses for an initially anisotropic material with its initial fabric being non-coaxial with the loading direction. Nevertheless, since there is no account for fabric evolution, the change of the degree of non-coaxiality with plastic deformation as evidenced by numerous experiments cannot be captured (Roscoe, 1970; Gao et al., 2014). Nemat-Nasser and Zhang (2002) has developed a micromechanically-based constitutive model based on an assumption that the deformation in granular materials is induced by relative sliding and rolling of particles. The study further employed a non-coaxial flow rule dependent on both fabric anisotropy and fabric change in the course of deformation. However, the predictive capability of the model remains to be testified to reproduce the typical non-coaxial sand behaviour observed in numerous torsional shear tests or simple shear tests.

In this study, a constitutive model for describing non-coaxial behaviour of granular materials will be proposed based on the anisotropic critical state theory (Li and Dafalias, 2012) wherein the role of fabric and fabric evolution is highlighted. In monotonic loading with fixed loading direction, a plastic potential explicitly expressed in terms of the invariants and joint invariants of the stress ratio tensor r_{ij} and a deviatoric fabric tensor F_{ij} is proposed. In conjunction with a fabric evolution law, the non-associated flow rule based on this plastic potential can naturally address the non-coaxial behaviour of granular materials under monotonic loading without significant rotation of principal stress directions. The plastic strain increment under rotation of principal stress axes is assumed to be dependent on the directions of the current stress, fabric and stress increment. The fabric is assumed to rotate towards the loading direction and to approach a magnitude proportional to a normalized stress ratio under rotation of principal stress axes. In the critical state, the predicted soil response becomes totally coaxial.

2. MODEL FRAMEWORK

Following Li and Dafalias (2004), we propose a hypoplasticity-like model in this paper to account for the accumulation of plastic deformation under rotation of principal stress directions and fabric evolution. The evolution of fabric with plastic deformation is considered in line with the anisotropic critical state theory (Li and Dafalias, 2012; Gao et al., 2014). The model is formulated in the space of stress ratio r_{ij} :

$r_{ij} = \left(\sigma_{ij} - p\delta_{ij}\right)/p = s_{ij}/p$, where σ_{ij} is the stress tensor, $p = \sigma_{ii}/3$ is the mean normal stress, δ_{ij} is the Kronecker delta ($\delta_{ij} = 1$ for $i = j$ and $\delta_{ij} = 0$ for $i \neq j$), and s_{ij} is the deviatoric stress. To facilitate a better understanding of our new model formulation, the model framework proposed by Li and Dafalias (2004) is briefly introduced.

The plastic shear strain increment is expressed as (Li and Dafalias, 2004)

$$de_{ij}^{p} = de_{ij}^{pm} + de_{ij}^{pt} = \langle L_m \rangle m_{ij} + \langle L_t \rangle \gamma_{ij} \tag{1}$$

where de_{ij}^{p} is the total plastic shear strain increment, de_{ij}^{pm} and de_{ij}^{pt} denote the plastic strain increment due to monotonic loading with fixed loading direction and due to rotation of principal stress directions, respectively; L_m and L_t are the corresponding loading indices; m_{ij} and γ_{ij} are traceless unit vectors defining the directions of plastic strain increment, $\langle\ \rangle$ are the Macauley brackets such that $\langle x \rangle = x$ for $x > 0$ and $\langle x \rangle = 0$ for any $x \leq 0$.

The total plastic volumetric strain increment $d\varepsilon_v^{p}$ is decomposed into one portion due to monotonic loading, $d\varepsilon_v^{pm}$, and the other portion due to rotation of principal stress directions, $d\varepsilon_v^{pt}$, as follows

$$d\varepsilon_v^{p} = d\varepsilon_v^{pm} + d\varepsilon_v^{pt} = \sqrt{\frac{2}{3}}\left(D_m\sqrt{de_{ij}^{pm}de_{ij}^{pm}} + D_t\sqrt{de_{ij}^{pt}de_{ij}^{pt}}\right) = \sqrt{\frac{2}{3}}\left(\langle L_m \rangle D_m + \langle L_t \rangle D_t\right) \tag{2}$$

where D_m ($= d\varepsilon_v^{pm} \Big/ \sqrt{2de_{ij}^{pm}de_{ij}^{pm}/3}$) and D_t ($= d\varepsilon_v^{pt} \Big/ \sqrt{2de_{ij}^{pt}de_{ij}^{pt}/3}$) denote the dilatancy relations for monotonic loading and rotation of principal stress directions, respectively. Notably, the decomposition of strain increment according to Eqs. (1) and (2) is merely for convenience of model development rather than yielding any solid physical significance. The main model formulations will be presented in the following section, while detailed derivations of the constitutive equations are shown in the Appendix.

3. MECHANICAL BEHAVIOUR OF SAND IN MONOTONIC LOADING

In the proposed model, the mechanical behaviour of sand in monotonic loading is described according to the classical plasticity theory, including key components governing the plastic potential, flue rule, yield function, dilatancy relation, hardening law and fabric evolution. In this paper, monotonic loading refers to the loading condition whereby the direction of principal stress remains unchanged while the shear strain keeps increasing. Typical examples include the conventional triaxial compression and extension. In some literature, such loading conditions are called proportional loading (e.g., Li and Dafalias, 2004).

3.1 Plastic potential and flow rule for monotonic loading

In order to model the non-coaxial sand behaviour in monotonic loading without significant of principal stress direction rotation, a plastic potential explicitly expressed in terms of the invariants and joint invariants of the r_{ij} and F_{ij} is employed. In conjunction with a law describing an evolving fabric, the non-associated flow rule based on this plastic potential can naturally address the non-coaxial behaviour of granular materials under such loading conditions.

The plastic potential g is expressed in terms of the fabric tensor F_{ij} and the stress ratio tensor r_{ij} as below

$$g = R/g(\theta) - H_g \exp\left[-k(A-1)^2\right] = 0 \tag{3}$$

with (Li and Dafalias, 2004)

$$g(\theta) = \frac{\sqrt{\left(1+c^2\right)^2 + 4c\left(1-c^2\right)\sin 3\theta} - \left(1+c^2\right)}{2(1-c)\sin 3\theta} \tag{4}$$

where $R = \sqrt{3/2 r_{ij} r_{ij}}$, c ($= M_e/M_c$) is the ratio between the critical state stress ratio in triaxial extension M_e and that in triaxial compression M_c, θ is the Lode angle, k is a positive model parameter, A is an anisotropic variable defined by a joint invariant of F_{ij} and n_{ij}, H_g is so defined as to render $g = 0$ according to current r_{ij} and F_{ij}. The plastic potential expressed by Eq. (3) borrows the expression of yield function used by Gao et al. (2014).

An important inclusion in the plastic potential function in Eq. (3) is a fabric anisotropy variable A defined by the following joint invariant between the fabric tensor F_{ij} and the loading direction tensor n_{ij} (see also Li and Dafalias, 2012; Gao et al., 2014)

$$A = F_{ij} n_{ij} \tag{5}$$

where F_{ij} is a symmetric, traceless tensor whose magnitude $F = \sqrt{F_{ij} F_{ij}}$ is referred to as the degree of fabric anisotropy. The definition of F_{ij} can be found in Li and Yu (2009, 2010) and Li and Dafalias (2012) which will not be repeated here. For convenience, F_{ij} is normalized such that F is unity at the critical state. For an initially cross-anisotropic sand sample with the $x-y$ plane being isotropic plane (typically the deposition plane) and the deposition direction aligning with the z-axis, the initial F_{ij} can be expressed as

$$F_{ij} = \begin{pmatrix} F_z & 0 & 0 \\ 0 & F_x & 0 \\ 0 & 0 & F_y \end{pmatrix} = \sqrt{\frac{2}{3}} \begin{pmatrix} F_0 & 0 & 0 \\ 0 & -F_0/2 & 0 \\ 0 & 0 & -F_0/2 \end{pmatrix} \tag{6}$$

where F_0 is the initial degree of fabric anisotropy. Note that in the above expression a coordinate system aligned with the direction of sample deposition has been assumed. If one chooses a coordinate system which is not aligned with the deposition direction of the sample, a corresponding orthogonal transformation is needed. The deviatoric unit loading direction tensor n_{ij} in Eq. (5) is defined as follows (Li and Dafalias, 2004)

$$n_{ij} = \frac{N_{ij} - N_{mm}\delta_{ij}/3}{\left\| N_{ij} - N_{mm}\delta_{ij}/3 \right\|} \tag{7}$$

with

$$N_{ij} = \frac{\partial f}{\partial r_{ij}} = \frac{\partial \left[R/g(\theta) \right]}{\partial r_{ij}} = \frac{1}{g(\theta)}\frac{\partial R}{\partial r_{ij}} - \frac{1}{g^2(\theta)}\frac{\partial g(\theta)}{\partial r_{ij}} \tag{8}$$

where f is the yield function the expression of which will be shown in Eq. (13) in the subsequent sections. Evidently, one has $n_{ii} = 0$ and $n_{ij}n_{ij} = 1$. A concrete derivation of the expression for N_{ij} can be found in Gao et al. (2014). Note that the loading direction n_{ij} here is defined as the normal to the yield surface or the gradient of the first portion of their plastic potential for simplicity. A more rigorous definition for n_{ij} can be based on the direction of plastic strain increment, as discussed in Li and Dafalias (2015) and Dafalias (2016).

A crucial ingredient to model the non-coaxial sand response hinges on an assumption that the fabric tensor F_{ij} used in Eq. (3) evolves with the plastic shear strain. In particular, based upon both experimental and micromechanical studies, the following fabric evolution law is employed for monotonic loading with fixed loading direction

(see also Gao et al., 2014)

$$dF_{ij}^{m} = \langle L_m \rangle \Theta_{ij} = \langle L_m \rangle \mu_1 \left(n_{ij} - F_{ij} \right) \tag{9}$$

where μ_1 is a positive model constant representing the rate of fabric evolution. The evolution law above is a simplified form of the one proposed by Li and Dafalias (2012). It renders F_{ij} rotates towards the loading direction n_{ij} to reach a magnitude of unity at the critical state.

By assuming a non-associated flow rule in the deviatoric stress space for monotonic loading, the plastic deviatoric strain increments de_{ij}^{pm} can be written as

$$de_{ij}^{pm} = \langle L_m \rangle m_{ij}\text{, with } m_{ij} = \frac{\partial g / \partial r_{ij} - \partial g / \partial r_{mm}\, \delta_{ij}/3}{\left\| \partial g / \partial r_{ij} - \partial g / \partial r_{mm}\, \delta_{ij}/3 \right\|} \tag{10}$$

From the plastic potential Eq. (1), one can get

$$\frac{\partial g}{\partial r_{ij}} = \underbrace{\frac{\partial \left[R / g(\theta) \right]}{\partial r_{ij}}}_{N_{ij}} + \underbrace{\frac{\partial g}{\partial A} \frac{\partial A}{\partial n_{kl}} \frac{\partial n_{kl}}{\partial r_{ij}}}_{\Pi_{ij}} \tag{11}$$

Since $\frac{\partial g}{\partial A} \frac{\partial A}{\partial n_{kl}} = \frac{2k(A-1)R}{g(\theta)} F_{kl}$ [Eq. (3)], Eq. (11) can be rewritten as

$$\frac{\partial g}{\partial r_{ij}} = \underbrace{\frac{\partial \left[R / g(\theta) \right]}{\partial r_{ij}}}_{N_{ij}} + \underbrace{\frac{2k(A-1)R}{g(\theta)} F_{kl} \frac{\partial n_{kl}}{\partial r_{ij}}}_{\Pi_{ij}} \tag{12}$$

By including fabric anisotropy in the plastic potential via the joint invariant A, $\frac{\partial g}{\partial r_{ij}}$ and m_{ij} can be expressed by two additive parts as shown in Eq. (12). The first part N_{ij} is apparently coaxial with the stress ratio tensor r_{ij} (or the stress tensor σ_{ij}). The second part Π_{ij} involving F_{ij} plays a unique role towards modelling the non-coaxial behaviour for sand. When the fabric tensor and stress tensor are initially coaxial and the loading direction does not change during the loading process, only the components of the fabric tensor will change while its principal axes of the fabric will not rotate during the loading process. In this case, F_{ij} and Π_{ij} will stay coaxial with r_{ij}, which gives rise to a prediction of coaxial soil behaviour. When the fabric and stress are initially non-coaxial, a non-coaxial strain will occur as $\Pi_{ij} \neq 0$ [Eq.(12)]. As the fabric evolves, F_{ij} rotates towards n_{ij} [Eq. (9)] and A increases [Eq. (5)], which leads to a reduction of magnitude for Π_{ij}. As a result, the portion of non-coaxial strain increment in the total plastic strain increment gradually decreases with the fabric evolution. At the critical state when $A=1$ and $F_{ij}=n_{ij}$, $\Pi_{ij}=0$, which indicates the non-coaxial strain increment totally vanishes. Such a model prediction is in agreement with both experimental observations and micromechanical studies (Gao et al., 2014). Note that the model also predicts a totally coaxial response for an isotropic sample with $F_{ij}=0$, because $F_{ij}=0$ makes $\Pi_{ij}=0$ in this case (Eq. 12).

3.2 Yield function and hardening law for monotonic loading

Though it is instructive to express the yield function for anisotropic granular materials in terms of both the stress tensor and fabric tensor (Li, 2013; Gao et al., 2014) which may help to describe the accumulation of plastic strain subjected to rotation of principal stress directions (Wang, 1970; Li, 2013), a fabric-independent yield function is used in the present study for the sake of simplicity. The expression of the yield function is assumed to be

$$f = R/g(\theta) - H = 0 \tag{13}$$

where H is a hardening parameter. The following evolution law for H is proposed

(Gao et al., 2014; Li and Dafalias, 2012):

$$dH = \langle L_m \rangle r_h = \langle L_m \rangle \frac{G(1-c_h e)}{pR}\left[M_c g(\theta)\exp(-n\zeta) - R\right] \tag{14}$$

where c_h and n are two positive model parameters; ζ is the dilatancy state parameter defined by Li and Dafalias (2012)

$$\zeta = \psi - e_A (A-1) \tag{15}$$

where e_A is a model parameter, $\psi = e - e_c$ is the state parameter defined by Been and Jefferies (1985) with e and e_c being the current void ratio and the critical state void ratio corresponding to the current mean normal stress p, respectively. In the present work, the critical state line in the $e-p$ plane is given by (Li and Wang, 1998)

$$e_c = e_\Gamma - \lambda_c (p/p_a)^\xi \tag{16}$$

where e_Γ, λ_c and ξ are material constants and p_a (=101 kPa) is the atmospheric pressure. Note that the expression of the critical state line in the $e-p$ plane is not fabric-dependent in this model. The dilatancy state parameter ζ expressed in terms of ψ and A is used to model effect of pressure, density and anisotropy on mechanical response of sand. In some models, a fabric-dependent expression for the critical state line has been used to render the state parameter ψ fabric-dependent (Wan and Guo, 2004).

Note also that Eq. (14) is used to obtain the plastic modulus which is a key part for the constitutive model (Eq. 36 in the Appendix). The final expression of the plastic modulus is the same as r_h which is similar to the one used in Li and Dafalias (2012). However, Li and Dafalias (2012) have not employed any explicit yield surface in their model, but assumed directly a plastic modulus dependent of the difference of R and a 'virtual' peak stress ratio that played the role of the bounding surface.

3.3 Dilatancy relation for monotonic loading

The following fabric-dependent dilatancy function for monotonic loading is used in this model (Li and Dafalias, 2012; Gao et al., 2014):

$$D_m = \frac{d_1}{M_c g(\theta)}\left[1 + \frac{R}{M_c g(\theta)}\right]\left[M_c g(\theta)\exp(m\zeta) - R\right] \tag{17}$$

where d_1 and m are two model constants. More detailed explanation of the dilatancy relation is given in Gao et al. (2014) and Li and Dafalias (2012).

4. MECHANICAL BEHAVIOUR OF SAND IN ROTATION OF PRINCIPAL STRESS DIRECTIONS

4.1 Tangential loading effect

The tangential loading effect needs to be properly considered to model the mechanical behaviour of soils subjected to pure rotation of principal stress directions if such a yield function as that expressed by Eq. (13) is to be used (Dafalias, 1986; Gutierrez et al., 1993; Hashiguchi and Tsutsumi, 2003; Li and Dafalias, 2004; Yu and Yuan, 2006; Nicot and Darve, 2007; Lashikari and Latifi, 2008). This is because L_m becomes 0 when dr_{ij} is orthogonal to n_{ij} [see Eq. (13)], whereas a real sand specimen may show significant accumulation of plastic deformation under such loading condition (e.g., Nakata et al., 1998). This essentially makes the model a hypoplastic type (Dafalias, 1986).

In the present model, the tangential loading effect is considered according to the following equation (Li and Dafalias, 2004)

$$\omega \chi_{ij} dr_{ij} - \langle L_t \rangle K_{pt} = 0 \tag{18}$$

where K_{pt} is the plastic modulus under pure rotation of principal stress directions, χ_{ij} is the tangential loading direction expressed as

$$\chi_{ij} = dr_{ij} - n_{kl} dr_{kl} n_{ij} \tag{19}$$

and

$$\omega = \left\langle 1 - \left[R / M_c g(\theta) \right]^{20} \right\rangle \tag{20}$$

Eq. (20) indicates that, when $R < M_c g(\theta)$, ω is approximately 1 and plastic strain occurs in rotation of principal stress directions. When $R > M_c g(\theta)$, however, $\omega = 0$ and the tangential loading effect vanishes as $L_t = 0$. Note that $\omega = 0$ at $R > M_c g(\theta)$ is assumed for the sake of simplicity, since no test data on pure stress axis rotation for sand with $R > M_c g(\theta)$ are available. As will be shown in the discussion of K_{pt} in the following section, the model gives infinite plastic shear strain increment under pure rotation of principal stress directions at $R = M_c g(\theta)$, which is consistent with the critical state theory. Note that the tangential loading direction χ_{ij} is defined based on the yield function for this model (Eq. 13). For other models with different expression for the yield function, χ_{ij} will be different.

4.2 Flow rule for pure rotation of principal stress axes

Much more significant non-coaxial deformation occurs when a sand specimen is subjected rotation of principal stress directions than monotonic loading with fixed loading direction (Gutierrez et al., 1993; Li and Yu, 2010). Hence, the flow rule for monotonic loading alone is not sufficient for modelling the mechanical behaviour of sand in rotation of principal stress directions. Past studies show that the flow rule for sand in rotation of principal stress directions can be expressed in terms of both the current stress state and the stress increment (Gutierrez et al., 1993; Nicot and Darve, 2007; Yu and Yuan, 2006; Lashikari and Latifi, 2008; Li and Dafalias, 2004; Hashiguchi and Tsutsumi, 2003). This approach will be followed in this paper, with special emphasis being placed on the role of fabric and fabric evolution. The flow rule for rotation of principal stress directions of this model is give as below

$$de_{ij}^{pt} = \langle L_t \rangle \gamma_{ij} = \langle L_t \rangle \frac{Bm_{ij} + B'n'_{ij}}{\left\| Bm_{ij} + B'n'_{ij} \right\|} \tag{21}$$

where

$$B = \left[R / M_c g(\theta) \right]^a \text{ and } B' = \langle 1 - B \rangle \tag{22}$$

$$n'_{ij} = \frac{\chi_{ij}}{\left\| \chi_{ij} \right\|} \tag{23}$$

where a is a positive model parameter. The McCauley brackets $\langle \ \rangle$ are used to prevent B' from becoming negative when $R > M_c g(\theta)$. Since n'_{ij} is orthogonal to n_{ij}, the non-coaxial deformation is mainly contributed by the term associated with n'_{ij}. Note that the term Bm_{ij} gives both coaxial and non-coaxial strain increments where the coaxial increment dominates. The expressions of B and B' are proposed on the basis of experimental observations that that the degree of non-coaxiality decreases as the stress ratio $R/g(\theta)$ increases (e.g., Gutierrez et al., 1993; Li and Yu, 2010). A unique feature of the flow rule expressed by Eq. (23) is that it accounts for the effect of anisotropy through incorporating m_{ij} which is fabric-dependent. This renders the plastic flow only coaxial at the critical state with both $R = M_c g(\theta)$ and $A = 1$, as

$B' = 0$ only when $R = M_c g(\theta)$ and m_{ij} is coaxial with n_{ij} (or r_{ij}) only when $R = M_c g(\theta)$ and $A = 1$. Such model responses are supported by experimental observations (Miura et al., 1986; Gutierrez et al., 1993; Yang et al., 2007).

4.3 Plastic modulus and dilatancy relation for rotation of principal stress directions

The plastic modulus and dilatancy relation are essential for modelling sand behaviour. Experimental data available in literature show that the mechanical behaviour of sand subjected to rotation of principal stress directions is dependent on various factors, including density, mean normal stress, fabric anisotropy, stress ratio and strain accumulation. There have been few attempts on developing comprehensive constitutive models to describe the mechanical behaviour of sand under pure rotation of principal stress directions. For instance, most of the existing models are not able to account for the effect of sand density. Li and Dafalias (2004) were among the first to propose a model for sand behaviour under rotation of principal stress directions in consideration of the effect of density and fabric anisotropy. The formulations used in this study are based on this work.

The plastic modulus for rotation of principal stress directions K_{pt} is given by

$$K_{pt} = \frac{G(h_1 - e)}{p_a F}\left[\frac{M_c g(\theta) - R}{R}\right] \tag{24}$$

where h_1 is a positive model parameters. Note that $K_{pt} = \infty$ when the soil fabric is isotropic with $F = 0$, and thus, no plastic deformation occurs under rotation of principal stress directions, which is in accordance with the expectation that the rotation of principal stress directions should not cause plastic deformation for an isotropic sand specimen. Since K_{pt} decreases as F increases, more plastic strain accumulates under otherwise identical conditions (Yang, 2013b). At the critical state, $R=M_c g(\theta)$ and $K_{pt}=0$, indicating that the plastic shear strain increment is infinite. This complies with the critical state theory.

Based on the work of Li and Dafalias (2004), the dilatancy relation for rotation of principal stress directions is proposed as follows

$$D_t=\frac{d_2 e^{d_3\zeta}}{g(\theta)}\frac{\left[M_c g(\theta)-R\right]}{e^{d_4\Omega}} \tag{25}$$

with

$$\Omega=\int K_{pt}L_t\sqrt{\Theta'_{ij}\Theta'_{ij}} \tag{26}$$

where d_2, d_3 and d_4 are three positive model parameters and Θ'_{ij} denotes the direction of fabric evolution under rotation of principal stress directions. The expression for Θ'_{ij} will be given in the subsequent sections. The term $g(\theta)$ at the denominator is used to make the sand response more contractive as the intermediate principal stress variable b increase (Yang et al., 2007; Tong et al., 2010). The dilatancy relation implies that there is no volumetric change at the critical state as $D_t=0$ when $R=M_c g(\theta)$. The presence of ζ makes the dilatancy relation dependent on density, mean effective stress and fabric anisotropy, as ζ is expressed in terms of both ψ and A. The term $\exp(d_4\Omega)$ is used to improve model prediction for volumetric change of sand in rotation of principal stress directions. It can be seen from Eqs. (25) and (26) that, in continuous rotation of principal stress directions with constant stress ratio $R/g(\theta)$, D_t gradually approaches 0 as Ω increases, an observation supported by experimental data (e.g., Nakata et al., 1998; Tong et al., 2010). Physically, this term implies that continuous fabric evolution due to rotation of principal stress directions (represented by $\sqrt{\Theta'_{ij}\Theta'_{ij}}$) makes the sand specimen stiffer (Li and Yu, 2010; Yang, 2013a).

4.4 Fabric evolution in rotation of principal stress directions

It remains difficult to measure fabric evolution in laboratory. Available knowledge on sand fabric evolution has been primarily acquired via micromechanics-based investigations such as those based on discrete element simulation (Li and Yu, 2010; Yang, 2013a; Fu and Dafalias, 2015). These simulations indicate that, under continuous rotation of principal stress directions, the fabric of sand always rotates towards the loading direction and approaches a constant magnitude after certain cycles. The final degree of anisotropy F is proportional to the stress ratio R . Based on such observations, the following fabric evolution law is proposed for rotation of principal stress directions

$$dF_{ij}^{t} = \langle L_t \rangle \Theta'_{ij} = \langle L_t \rangle \mu_2 \left[\frac{R}{M_c g(\theta)} n_{ij} - F_{ij} \right] \tag{27}$$

where μ_2 is a positive model parameter.

5. ELASTIC MODULI AND INCREMENTAL ELASTIC RELATION

As plastic strain typically dominates sand deformation, the effect of anisotropy on elasticity of sand is considered negligible in this model (though it can be taken into account in a consistent manner with the proposed framework according to Zhao and Gao, 2016). The following isotropic pressure-dependent elastic stress strain relations (Richart et al., 1970, Li and Dafalias, 2004, 2012) are employed

$$G = G_0 \frac{(2.97 - e)^2}{1+e} \sqrt{pp_a} \tag{28}$$

$$K = G \frac{2(1+\nu)}{3(1-2\nu)} \tag{29}$$

where G and K denote the elastic shear and bulk modulus, respectively, G_0 is a material constant, e is the void ratio and ν is the Poisson's ratio assumed to be a constant. In conjunction with Eqs. (28) and (29), the following hypoelastic relation is assumed for calculating the incrementally reversible deviatoric and volumetric strain increments de_{ij}^e and $d\varepsilon_v^e$:

$$de_{ij}^e = \frac{ds_{ij}}{2G} \text{ and } d\varepsilon_v^e = \frac{dp}{K} \tag{30}$$

6. MODEL SIMULATIONS

Test data on Toyoura sand are used to verify the predictive capability of the proposed model. The tests to be used for the verification include the undrained simple shear tests on dry-deposited Toyoura sand reported by Yoshimine et al. (1998), the drained tests with continuous rotation of principal stress directions on Toyoura sand prepared by Multiple Seiving Pluviation (MSP) method by Miura et al. (1986) and the undrained tests with continuous rotation of principal stress directions on Toyoura sand prepared by MSP method by Nakata et al. (1998).

The determination of model parameters for monotonic loading with fixed loading direction has been discussed in Gao et al. (2014) which will not be repeated. Only the method for determining the parameters associated with rotation of principal stress directions will be provided here. Under pure rotation of principal stress directions, the sand fabric changes fast as it keeps rotating with the principal stress directions (Li and Yu, 2010; Fu and Dafalias, 2015). Therefore, the parameter μ_2 is typically big and a default value of 1000 can be used. The parameters h_1 and a should be determined using the stress-strain relation of sand in drained rotation of principal stress directions. h_1 affects the sand stiffness and a describes the degree of non-coaxiality. The parameters d_2, d_3 and d_4 have significant influence on the dilatancy of sand in rotation of principal stress directions. They should be determined by trial and error using the test results under undrained rotation of principal stress directions. The parameters determined for Toyoura sand are listed in Table 1. The same initial degree of anisotropy F_0 is assumed for Toyoura sand prepared by both dry-deposition and MSP methods.

6.1 Model simulation for sand behaviour in monotonic loading

A sand sample may show non-coaxial response in monotonic loading when the initial fabric is anisotropic (e.g., Gutierrez et al., 1993; Rodriguez and Lade, 2014; Gao et al., 2014; Zhao and Guo, 2015). The present model can describe such sand behaviour using a flow rule involving fabric tensor [Eq. (10)].

Table 1 Model parameters for Toyoura sand

Elasticity	Critical state	Monotonic loading	Rotation of principal stress directions	Initial degree of anisotropy
G_0=125 ν=0.2	M_c=1.25 c=0.75 e_Γ=0.934 λ_c=0.019 ξ=0.7	k=0.03 c_h=0.9 n=3.0 d_1=0.2 m=5.3 e_A=0.1 μ_1=5.7	h_1=5.02 a=2.0 d_2=4.14 d_3=3.94 d_4=0.00042 μ_2=1000.0	F_0=0.45

Fig. 1 shows the model response for dry-deposited Toyoura sand in undrained simple shear tests. More details of the test procedure can be found in Yoshimine et al. (1998). In the figures, σ_1 is the major principal stress, σ_3 is the minor principal stress, ε_1 is the major principal strain, ε_3 is the minor principal strain, K_0 is the initial value of σ_3/σ_1, α is the angle between the vertical direction and major principal stress direction and $\alpha(d\varepsilon)$ is the angle between the vertical direction and major principal strain increment. Notably, the model offers good predictions on the stress and stain relation, effective stress paths and non-coaxial response for both tests. Note that $\alpha(d\varepsilon)$ is always 45° for both tests (Figs. 1e and f). For the test with an initial isotopic stress state ($K_0 = 1$), α first decreases to a minimum value around 40° and then gradually approaches $\alpha(d\varepsilon)$ (Fig. 1e). In the case with an initially anisotropic stress state ($K_0 = 0.5$), α increases steadily with the $\varepsilon_1 - \varepsilon_3$ and approaches $\alpha(d\varepsilon)$ (Fig. 1e). Such a trend is well captured by the model (Fig. 1f). The reduced difference between $\alpha(d\varepsilon)$ and α is due to fabric evolution. When the samples reach the critical state with infinite $\varepsilon_1 - \varepsilon_3$, $R = M_c g(\theta)$ and $A = 1$, the non-coaxial strain increment vanishes and α will reach 45°. To demonstrate the role of a fabric-dependent plastic potential in modelling non-coaxial sand response in simple shear, model simulations with $k = 0$ (rendering the plastic potential fabric-independent) are presented in Fig. 1g. It is evident that, for the sample with K_0=1, the simulated α reaches 45^{o} at the very beginning of the test, while the test data shows that α first decreases to 40^{o} and then recovers gradually towards 45^{o}. The simulation in Fig. 1g also shows that α reaches 45^{o} when the shear strain is about 1% for the sample with K_0=0.5, while the experimental data indicate that this cannot happen until the shear strain is much larger than 14%. This indicates that a fabric-dependent plastic potential is indeed crucial for modelling the non-coaxial sand response in simple shear.

Fig. 2 shows the model simulation for sand in drained torsional shear tests with constant b and α, where $b=(\sigma_2-\sigma_3)/(\sigma_1-\sigma_3)$ is the intermediate principal stress variable with σ_2 being the intermediate principal stress. The model gives lower shear modulus (Fig. 2a) and more contractive response (Fig. 2b) as α increases, which is in agreement with experimental observations (Miura et al., 1986; Yoshimine et a., 1998). Fig. 2 (c) indicates that $\alpha(d\varepsilon)=\alpha$ when $\alpha=0^\circ$ and $\alpha=90^\circ$, which is also observed in laboratory tests on various types of sand (Miura et al., 1986; Gutierrez et al., 1993; Yoshimine et al, 1998; Rodriguez and Lade, 2014). The coaxial response is induced by the change of magnitude of fabric tensor only without any change in the principal axes of the fabric in the cases of $\alpha=0^\circ$ and $\alpha=90^\circ$. In all the other cases when α is between 0° and 90°, coaxiality is predicted at relatively low $\sigma_1-\sigma_3$ due to the employment of isotropic elastic relation in Eq. (30). Beyond this elastic stage, a distinct difference between $\alpha(d\varepsilon)$ and α in the order of 5 to 8 degrees is found as shown in Fig. 2(c), which signals a clear non-coaxiality. From a practical perspective, the 5-8 degrees of non-coaxiality may not appear to be particularly significant. It is however important from a theoretical point of view. Upon further loading, the fabric tends to rotate towards the direction of stress, and the difference between $\alpha(d\varepsilon)$ and α predicted by the model decreases, and the non-coaxiality will totally disappear at the critical state. Notably, the model gives $\alpha(d\varepsilon)\geq\alpha$ for all the tests, which is supported by both experimental tests (Symes et al., 1988; Yoshimine et al., 1998; Yang, 2013b) and micromechanical studies (Li and Yu, 2009; Yang, 2013a; Li and Yu, 2015; Yang et al., 2015). Fig. 2d shows the model simulation for non-coaxial sand response with a fabric-independent plastic potential ($k=0$). It can be seen that the model gives $\alpha(d\varepsilon)=\alpha$ in this case, which is apparently not in agreement with experimental observations.

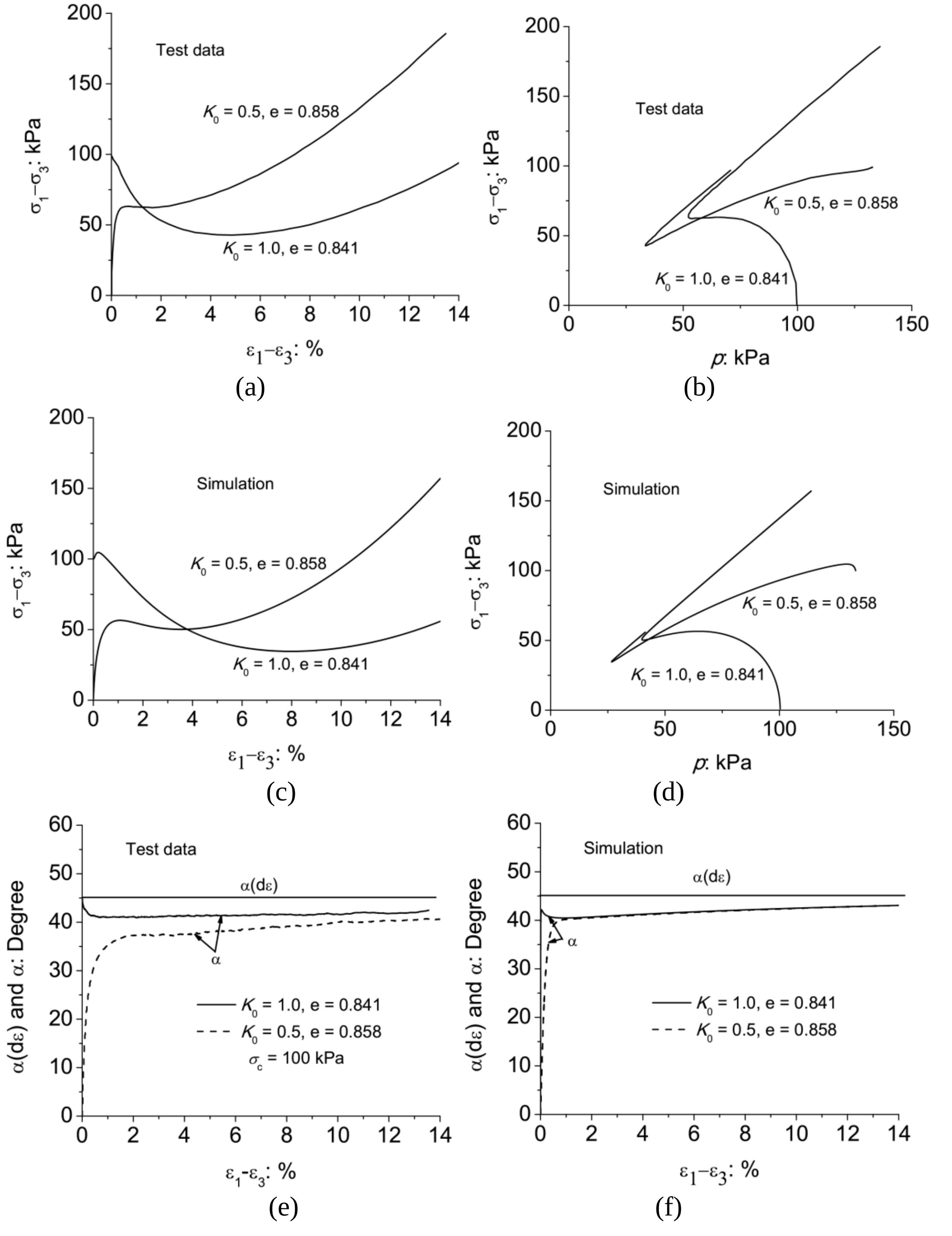

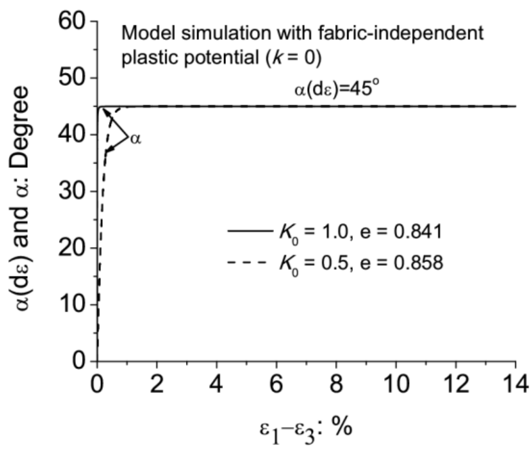

(g)

Fig. 1 Comparison between experimental results (a, b, e) and model simulations (c, d, f) for mechanical behaviour of dry-deposited Toyoura sand in undrained simple shear tests (test data from Yoshimine et al., 1998) and illustration of effect of fabric-dependent plastic potential for modelling non-coaxial sand response (g)

6.2 Model simulation for sand behaviour in continuous rotation of principal stress directions

Miura et al. (1986) performed a series of drained hollow cylinder torsional shear tests on Toyoura sand prepared by MSP method. During their tests, the principal stress directions were rotated continuously at constant p, constant b and constant mobilized friction angle φ_m [$\sin\varphi_m = (\sigma_1 - \sigma_3)/(\sigma_1 + \sigma_3)$]. The samples were proportionally loaded to the prescribed p, b and φ_m before the application of principal stress direction rotation. In Figs. 3-10, D_r is the relative density of sand after pre-shearing and before the rotation of principal stress direction.

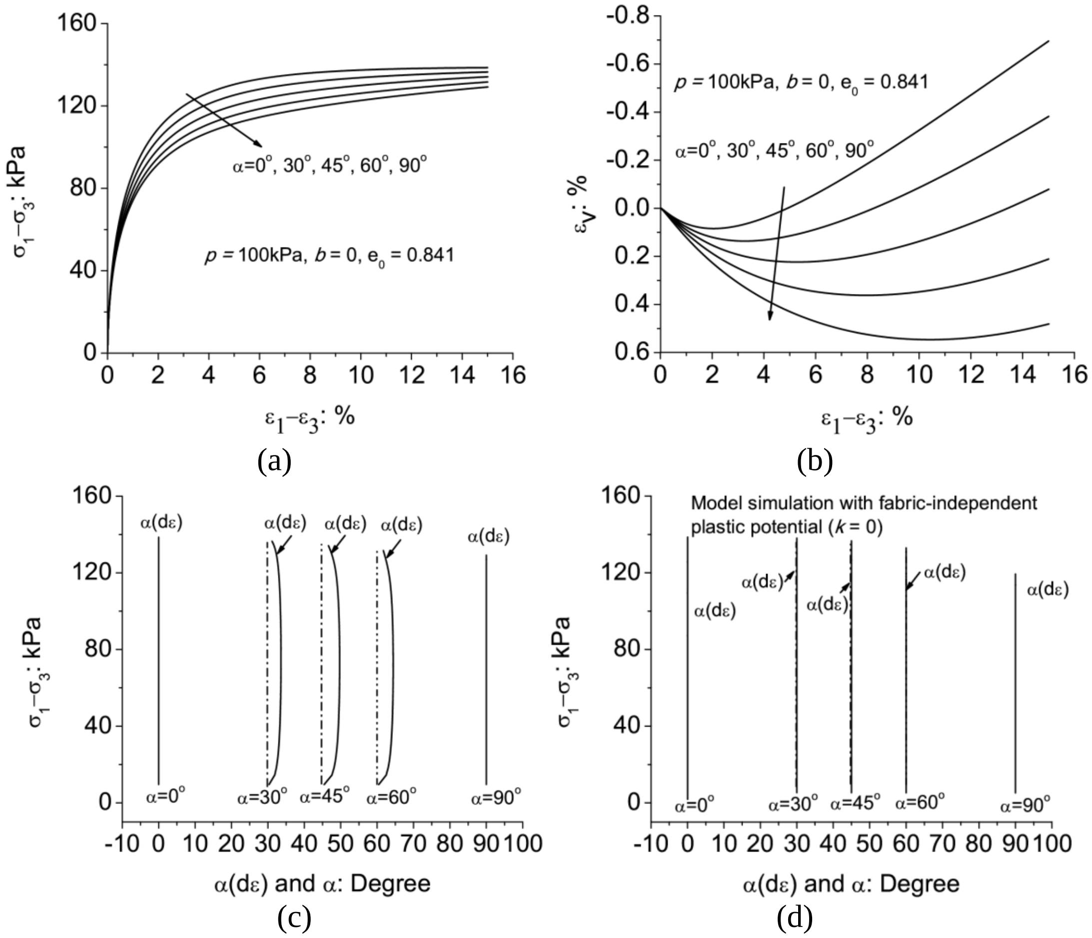

Fig. 2 Model simulation for stress strain relation (a and b) and non-coaxial sand response in drained torsional shear tests with constant α and b (c); (d) Model simulation for non-coaxial sand response with fabric-independent plastic potential

The experimental results and model simulations for the strain developments of two of the tests are compared in Fig. 3 (initial $\alpha = 0^\circ$) and Fig. 4 (initial $\alpha = 90^\circ$). While the model provides rather good predictions for the axial strain ε_a, the circumferential strain ε_θ and the shear strain $\varepsilon_{a\theta}$, it overestimates the radial strain ε_r. Figs.3 c and d also show the evolution of volumetric strain in 7 cycles of R1+0^o test. The model can capture the increase of volumetric strain with number of cycles but overestimates the maximum volumetric change. Fig. 5a shows the $\varepsilon_{a\theta} - (\varepsilon_a - \varepsilon_\theta)/2$ relation for four tests with different initial α (p , b and φ_m are the same). Fig. 5b shows the corresponding model simulations for the strain paths. Evidently, the model predictions capture the general trend of the strain paths for the sand. The maximum discrepancy between the model predictions and test data is observed for the R1+90° test (initial $\alpha = 45^\circ$). Indeed, the strain distribution in a real sand test is commonly non-uniform, whereas the model simulations have been based on a uniform-strain assumption for a sample. This may be attributable to the observed discrepancy.

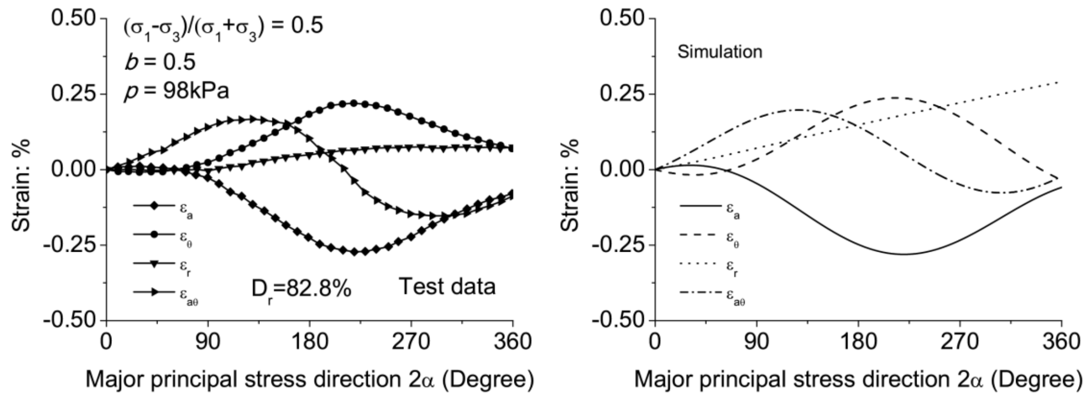

(a) (b)

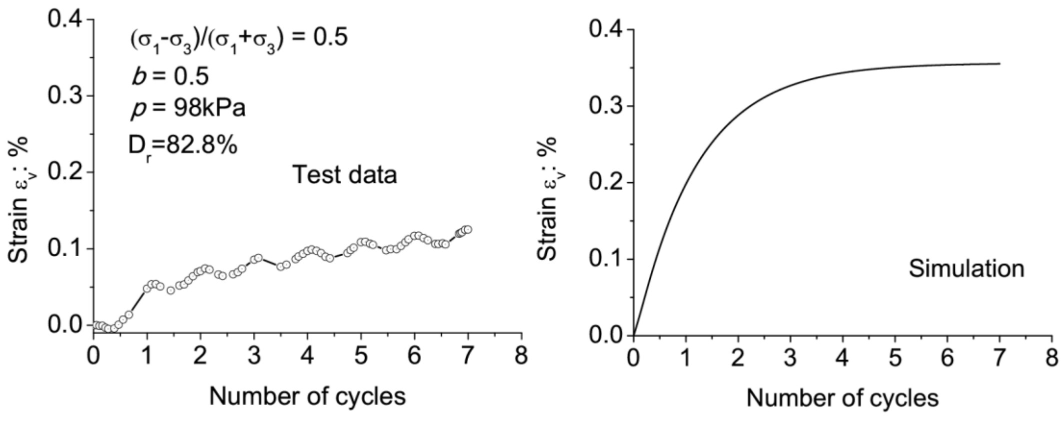

(c) (d)

Fig. 3 Experimental data (a, c) and model simulation (b, d) of strain evolution in drained torsional shear tests (R1+0° test, test data from Miura et al., 1986)

Figs. 6 and 7 show the experimental results and model simulations for the degree of non-coaxiality denoted by $\alpha(d\varepsilon)-\alpha$ in the R1+0^o test and the R1-90^o test. The model offers satisfactory estimations on the degree of non-coaxiality for both cases. However, it does not perform equally well in capturing the periodical variation of $\alpha(d\varepsilon)-\alpha$, since the model gives constant $\alpha(d\varepsilon)-\alpha$ after the major principal stress direction has changed about 45^o. As show by Lashkari and Latifi (2008), in order to capture the periodic variation of $\alpha(d\varepsilon)-\alpha$, one has to assume that the plastic strain increment is dependent on the major principal stress direction α. However, such model formulation does not satisfy the requirement of objectivity as α is not an objective quantity. Further studies need to be devoted to identifying the micromechanical mechanism for the periodic variation of $\alpha(d\varepsilon)-\alpha$. Better model formulations for modelling the non-coaxial response may be proposed based on such mechanism.

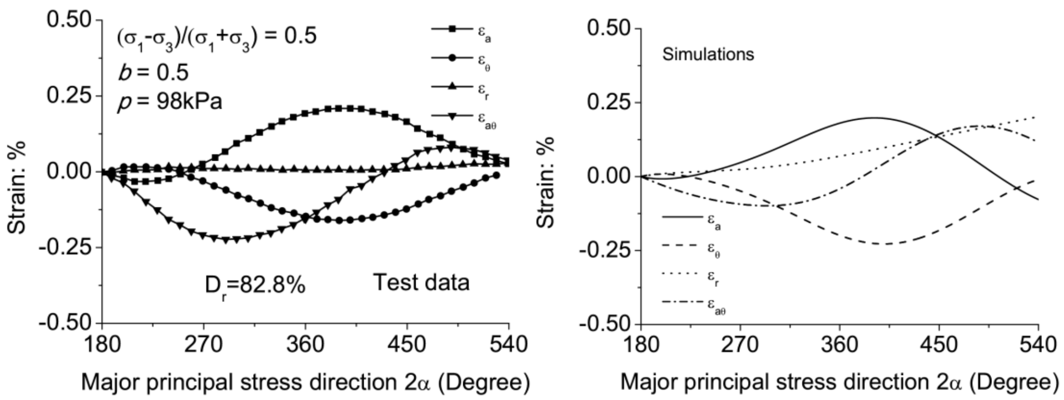

(a) (b)

Fig. 4 (a) Experimental data and (b) model simulation of the relation between strains and direction of principal stress (R1+180^o test, data from Miura et al., 1986)

A serious of undrained torsional shear tests with continuous rotation of principal stress directions have been carried out by Nakata et al. (1998) on Toyoura sand prepared by the MSP method. The initial confining pressure p_c was 100 kPa and the intermediate principal stress variable was $b = 0.5$. Before the application of principal stress direction rotation, the samples were first proportionally loaded to a prescribed p_c and q ($= \sqrt{3/2 s_{ij} s_{ij}}$) with $b = 0.5$ under drained loading condition.

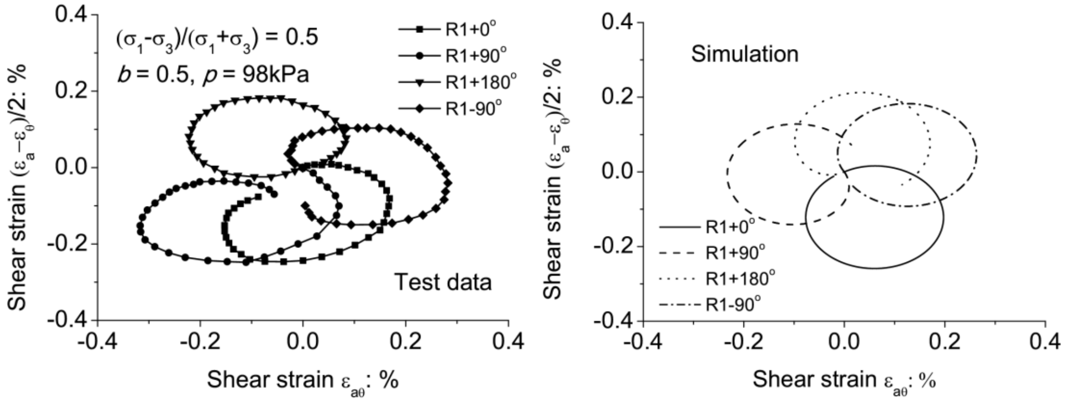

(a) (b)

Fig. 5 (a) Experimental data and (b) model simulation of the strain paths under rotation principal stress direction (test data from Miura et al., 1986)

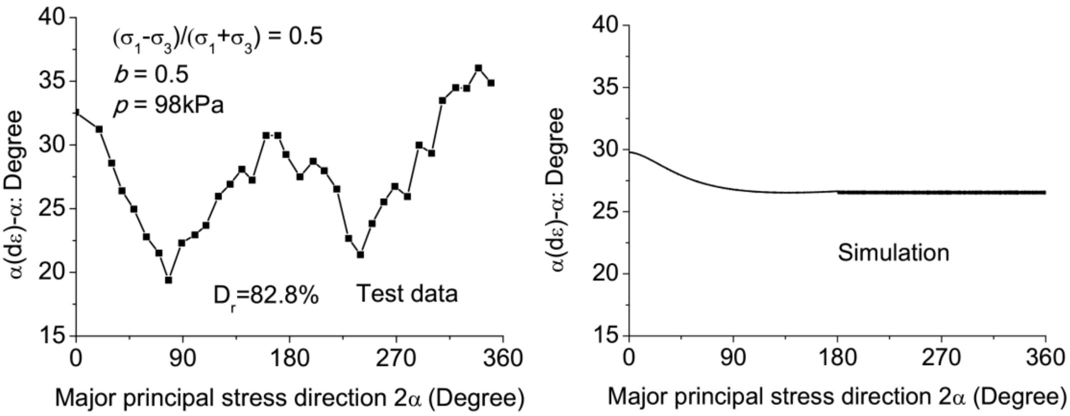

(a) (b)

Fig. 6 (a) Experimental data and (b) model simulation of the angles of non-coaxiality ($R1+0^o$ test, test data from Miura et al., 1986)

Figs. 8 and 9 show the measured and simulated strain components (axial strain ε_a, circumferential strain ε_θ and shear strain $\varepsilon_{a\theta}$ and radial strain ε_r) as well as the excess pore pressure u against the number of cycles of stress rotation. The model predicts the evolution of excess pore pressure reasonably well for both samples. The simulated strain development captures the general trend but is less accurate than for the excess pore pressure. A possible reason may be that the model assumes a uniform deformation for the sample, but the actual strain distribution inside the sample can be highly non-uniform.

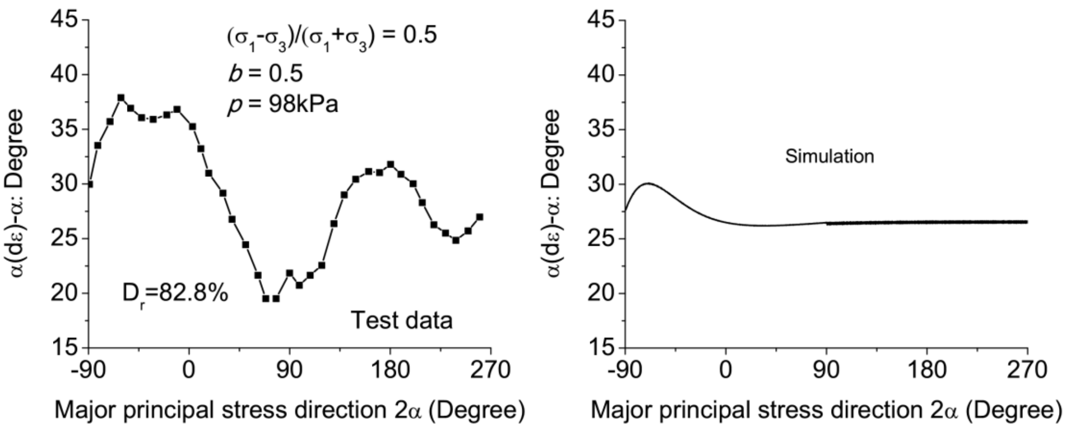

(a) (b)

Fig. 7 (a) Experimental data and (b) model simulation of the angles of non-coaxiality (R1-90^o test, test data from Miura et al., 1986)

6.3 Fabric evolution in continuous rotation of principal stress directions

It is instructive to trace the evolution of fabric evolution during the loading process and to assess its impact on the mechanical response of sand. In Gao et al. (2014), we have demonstrated how the model captures the fabric evolution in monotonic loading with fixed loading direction. This section will be devoted to the case of rotation of principal stress direction. Fig. 10 shows the simulated fabric evolution under pure rotation of principal stress directions. The loading condition is identical to the R1+0^{o} test performed by Miura et al. (1986). In the figure, $\alpha\left(F_{ij}\right)$ denotes the angle between the vertical direction and the major principal fabric direction. Fig. 10a indicates that both the degree of anisotropy F and the anisotropic variable A increase at the initial loading stage and then gradually become constant after the major principal stress direction has changed by about 70 ^{o}. Evidently, the fabric rotates with the rotation of the principal stress direction, but its magnitude stays unchanged. It can be seen from Fig. 10b that the angle between the directions of the major principal stress and major principal fabric, denoted by $\alpha-\alpha\left(F_{ij}\right)$, increases at the initial loading stage, indicating the change of fabric change is lagging behind the stress change due to the passive nature of former. When α reaches about 70^{o}, $\alpha-\alpha\left(F_{ij}\right)$ becomes constant. The simulated fabric evolution is similar to the distinct element simulations by Fu and Dafalias (2015).

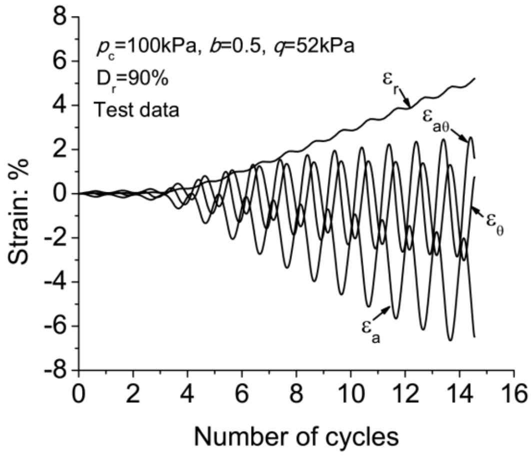

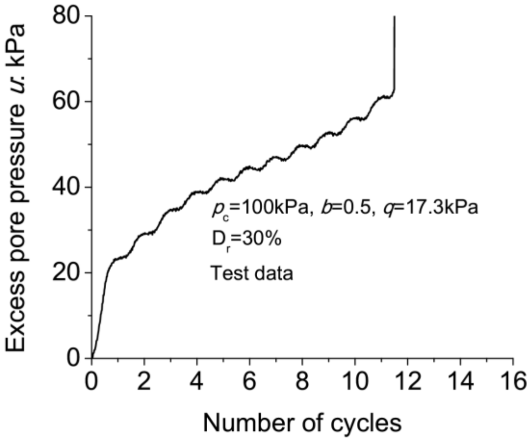

(a) (b)

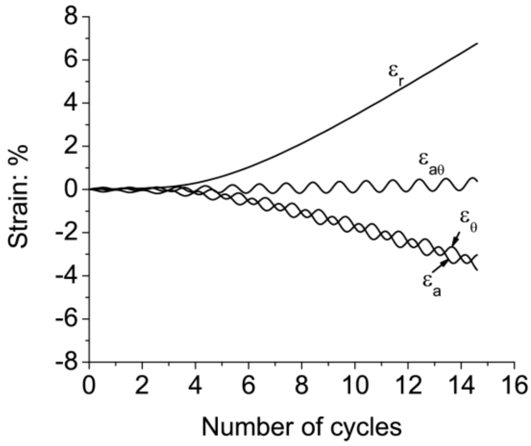

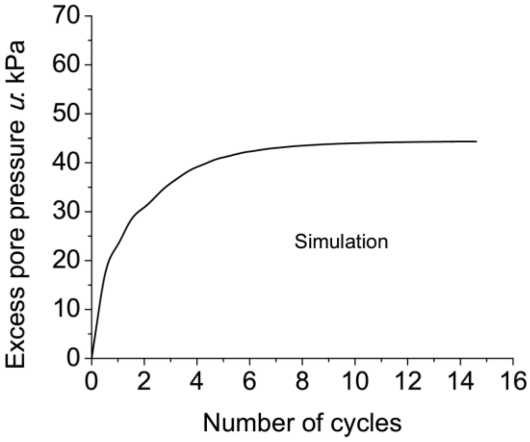

(c) (d)

Fig. 8 Experimental results (a and b) and model simulations (c and d) for strain components and excess pore pressure against number of cycles of rotation (D_r=90%, test data from Nakata et al., 1998)

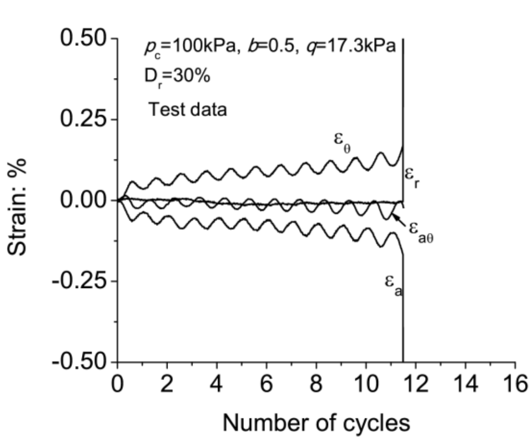

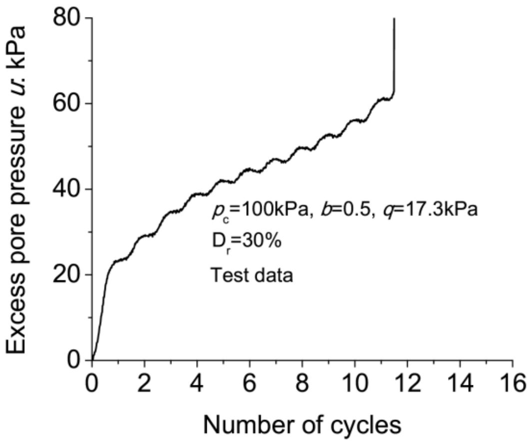

(a) (b)

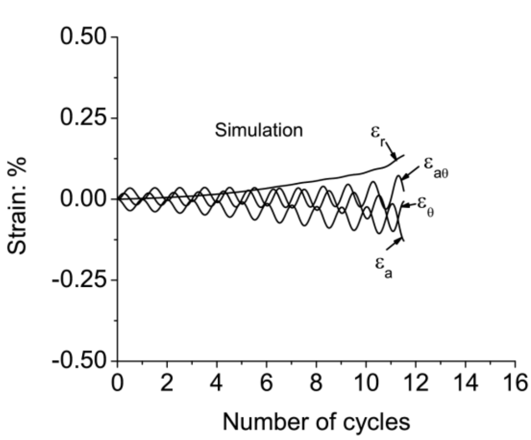

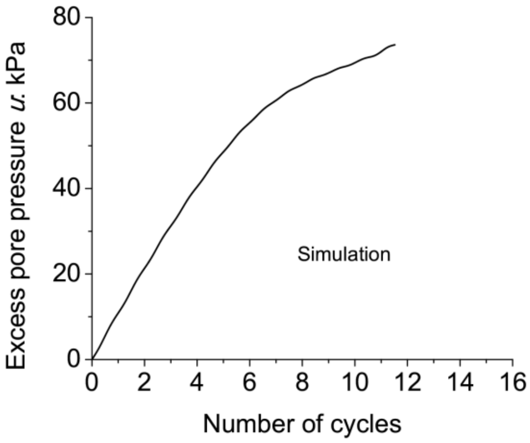

(c) (d)

Fig. 9 Experimental results (a and b) and model simulations (c and d) for strain components and excess pore pressure against number of cycles of rotation (D_r=30%, test data from Nakata et al., 1998)

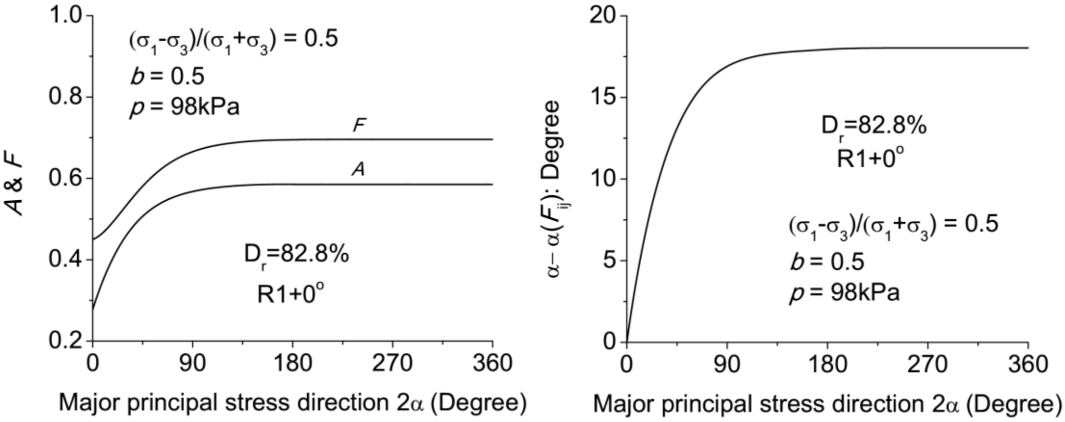

(a) (b)

Fig. 10 Model simulation of fabric evolution in drained rotation of principal stress directions

7. CONCLUSION

Granular materials may show non-coaxial response due to fabric anisotropy. Micromechanical studies indicate that proper consideration of fabric and fabric evolution is crucial for modelling the non-coaxial sand response. A new constitutive model has been proposed to simulate the non-coaxial sand behaviour. The model is formulated within the framework of the anisotropic critical state theory (Li & Dafalias, 2012; Gao et al., 2014) and highlights the key role played by sand fabric and its evolution in dictating the non-coaxial shear behaviour in sand. The proposed model contains the following main features:

(a) A plastic potential explicitly expressed in terms of the fabric tensor. In conjunction with the fabric evolution law, it enables the non-coaxial response of sand in monotonic loading with fixed loading direction to be conveniently and faithfully captured.

(b) A dependence of plastic strain increment on the current stress state, the direction of stress increment and the current fabric in rotation of principal stress directions. This feature renders the model predicts a relatively stronger non-coaxial response when the stress ratio is low and the degree of fabric anisotropy is high. The sand response becomes coaxial at the critical state when the fabric is co-directional with the loading direction and reaches its critical state value.

(c) A fabric evolution law dependent on the plastic deviatoric strain. According to such a law, in monotonic loading, the fabric reaches a constant magnitude and becomes co-directional with the loading direction at the critical state. When the sand sample is subjected to rotation of principal stress directions, the fabric always rotate towards the loading direction and approach a constant magnitude dependent on the stress ratio.

(d) Both the plastic modulus and dilatancy relation dependent on the fabric and fabric evolution for rotation of principal stress directions. It is further assumed that no plastic deformation is produced in principal stress direction rotation when a sand sample has isotropic fabric.

The model has been employed to simulate the mechanical behaviour of Toyoura sand, and the model predictions have been well verified by test results under both monotonic loading and rotation of principal stress directions. Notably, the present model employs a yield function independent of the fabric, and therefore, the tangential loading effect must be considered separately to model sand response subjected to rotation of principal stress directions. The representation theorem for tensor-valued isotropic functions (Wang, 1970) indicates that proper yield function and plastic potential function expressed in terms of the stress tensor and σ_{ij}, fabric tensor F_{ij} and other internal variables can lend both mathematical rigor and physical soundness in constitutive modelling of anisotropic sand (Li, 2013; Li and Dafalias, 2015; Dafalias, 2016). Indeed, the energy dissipation in anisotropic granular materials is inherently associated with the sand fabric and its evolution during the loading process. If a fabric-dependent yield function and a fabric-dependent plastic potential can be found appropriate for both monotonic loading and pure rotation of principal stress axes,, with further consideration of fabric evolution, a more consistent model can be developed to offer a unified description of non-coaxial sand behaviour in a more natural way. Future work will be done in this regard.

It is noteworthy that the presented formulation makes the model incrementally nonlinear, and its numerical implementation in finite element method is rather challenging. Most implicit stress integration methods require explicit second derivatives of the yield function/ the plastic potential function, which proves to be difficult for the present model especially in the case of principal stress rotation. In this regard, it is advisable to employ the explicit stress integration method with automatic sub-stepping proposed by Sloan et al. (2001). This explicit integration method is able to handle highly nonlinear constitutive relations by subdividing each loading step automatically and adaptively according to its degree of nonlinearity. The method has been demonstrated by Zhao et al. (2005) to suit for a wide range of complex soil models, with reasonable efficiency, accuracy and robustness. Hence it is advisable to employ this stress integration method to implement the present model in FEM for practical boundary value problem simulations.

APPENDIX: THE CONSTITUTIVE EQUATIONS

According to the elastic stress strain relation and equations for the plastic strain increment, one can get

$$\begin{aligned} d\sigma_{ij} &= E_{ijkl} d\varepsilon_{kl}^{e} = E_{ijkl}\left(d\varepsilon_{kl} - d\varepsilon_{kl}^{p}\right) = E_{ijkl}\left(d\varepsilon_{kl} - d\varepsilon_{kl}^{pm} - d\varepsilon_{kl}^{pt}\right) \\ &= E_{ijkl}\left[d\varepsilon_{kl} - \langle L_m \rangle x_{kl} - \langle L_t \rangle x'_{kl}\right] \end{aligned} \tag{31}$$

where E_{ijkl} is the elastic stiffness tensor expressed as

$$E_{ijkl} = \left(K - 2G/3\right)\delta_{ij}\delta_{kl} + G\left(\delta_{ki}\delta_{lj} + \delta_{li}\delta_{kj}\right) \tag{32}$$

and

$$x_{ij} = m_{ij} + \frac{1}{3}\sqrt{\frac{2}{3}} D_m \delta_{ij} \tag{33}$$

$$x'_{ij} = \gamma_{ij} + \frac{1}{3}\sqrt{\frac{2}{3}} D_t \delta_{ij} \tag{34}$$

The condition of consistency for the yield function Eq. (13) can be expressed as

$$df = \frac{\partial f}{\partial r_{kl}} \frac{\partial r_{kl}}{\partial \sigma_{ij}} d\sigma_{ij} - \langle L_m \rangle \frac{\partial f}{\partial H} r_h = \frac{\partial f}{\partial \sigma_{ij}} d\sigma_{ij} - \langle L_m \rangle K_{pm} = 0 \tag{35}$$

where

$$K_{pm} = -\frac{\partial f}{\partial H} r_h = r_h \tag{36}$$

The loading mechanism for rotation of principal stress directions can be written as

$$\underbrace{\omega \chi_{kl} \frac{\partial r_{kl}}{\partial \sigma_{ij}}}_{C_{ij}} d\sigma_{ij} - \langle L_t \rangle K_{pt} = 0 \tag{37}$$

Substituting Eqs. (33) and (34) into Eq. (35), one can get

$$\frac{\partial f}{\partial \sigma_{ij}}\left[d\varepsilon_{ij}-\langle L_m\rangle x_{ij}-\langle L_t\rangle x'_{ij}\right]-\langle L_m\rangle K_{pm}=0 \tag{38}$$

Eq. (37) can be rewritten as below based on Eqs. (33) and (34)

$$C_{ij}\left[d\varepsilon_{ij}-\langle L_m\rangle x_{ij}-\langle L_t\rangle x'_{ij}\right]-\langle L_t\rangle K_{pt}=0 \tag{39}$$

Combing Eqs. (38) and (39), the expression for L_m and L_t can be got as below

$$L_m=\frac{C_{ij}-C_{cd}x_{cd}\dfrac{\partial f}{\partial \sigma_{ij}}\Big/\left(\dfrac{\partial f}{\partial \sigma_{pq}}x_{pq}+K_{pm}\right)}{K_{pt}-C_{pq}x_{pq}\dfrac{\partial f}{\partial \sigma_{cd}}x'_{cd}\Big/\left(\dfrac{\partial f}{\partial \sigma_{pq}}x_{pq}+K_{pm}\right)}d\varepsilon_{ij}=\Pi_{ij}d\varepsilon_{ij} \tag{40}$$

$$L_t=\frac{\dfrac{\partial f}{\partial \sigma_{ij}}-\dfrac{\partial f}{\partial \sigma_{cd}}x'_{cd}\Pi_{ij}}{\dfrac{\partial f}{\partial \sigma_{pq}}x_{pq}+K_{pm}}d\varepsilon_{ij}=\mathrm{H}_{ij}d\varepsilon_{ij} \tag{41}$$

Substituting Eq. (40) and (41) into Eq. (31), the constitutive equation can be obtained as below

$$d\sigma_{ij}=\Lambda_{ijkl}d\varepsilon_{ij} \tag{42}$$

$$\Lambda_{ijkl}=E_{ijkl}-h(L_m)E_{ijmn}x_{mn}\Pi_{kl}-h(L_t)E_{ijmn}x'_{mn}\mathrm{H}_{kl} \tag{43}$$

where $h(L)$ is the Heaviside step function, with $h(L>0)=1$ and $h(L\le 0)=0$.

NOTATION

A anisotropic variable

b intermediate principal stress parameter

D_m , D_{pt}	dilatancy equation for monotonic loading and rotation of principal stress direction
D_r	relative density
e, e_c	void ratio and critical state void ratio
$\varepsilon_{ij}^e, \varepsilon_{ij}^p$	elastic and plastic strain
F_{ij}	deviatoric void fabric tensor
f	yield function
G	elastic shear modulus
$g(\theta)$	interpolation function for the critical state stress ratio
K	elastic bulk modulus
K_{pm}, K_{pt}	plastic modulus for monotonic loading and rotation of principal stress direction
M_c, M_e	critical state stress ratio in triaxial compression and triaxial extension
p	mean stress
R	stress ratio
r_{ij}	stress ratio tensor
s_{ij}	deviatoric stress tensor
α	angle between the major principal stress and direction of deposition
δ_{ij}	Kronecker delta
$\varepsilon_1, \varepsilon_2, \varepsilon_3$	major, intermediate and minor principal strain respectively
$\varepsilon_z, \varepsilon_r, \varepsilon_z, \varepsilon_{z\theta}$	axial stress, radial, axial stress and shear strain
θ	Lode angle of the stress tensor
σ_1, σ_2, σ_3	major, intermediate and minor principal stress respectively

σ_{ij}	stress tensor
$\sigma_z, \sigma_r, \sigma_z, \sigma_{z\theta}$	axial stress, radial, axial stress and shear stress
ψ	state parameter

REFERENCES

Been, K., Jefferies, M.G., 1985. A state parameter for sands. Géotechnique 35 (2): 99-112.

Darve, F., 1974. Contribution a la Determination de la Loi Rehologique Incrementale des Sols. Thesis presented to the Universite de Grenoble, at Grenoble, France, in partial fulfilment of the requirements for the degree of Doctor of Philosophy.

Dafalias, Y.F., 1975. On Cyclic and Anisotropic Plasticity. Thesis presented to the University of California, at Berkeley, Calif., in partial fulfilment of the requirements for the degree of Doctor of Philosophy.

Dafalias, Y.F., Popov, E.P., 1977. Cyclic Loading for Materials with a Vanishing Elastic Region," Nuclear Engineering and Design, 41, 293-302.

Dafalias, Y.F., 1986. Bounding surface plasticity. I: Mathematical foundation and hypoplasticity. J. Eng. Mech. 112 (9), 966-987.

Dafalias, Y. F., 2016. Must critical state theory be revisited to include fabric effects? Acta Geotechnica. 11 (3), 479-491.

Fu, P., Dafalias, Y.F., 2015. Relationship between void- and contact normal-based fabric tensors for 2D idealized granular materials. Int. J. Solids Struct. 63, 68-81.

Gao, Z., Zhao, J., 2013. Strain localization and fabric evolution in sand. Int. J. Solids Struct. 50(22-23), 3634-3648.

Gao, Z., Zhao, J., Li, X.S., Dafalias, Y.F., 2014. A critical state sand plasticity model accounting for fabric evolution. Int. J. Numer. Anlyt. Meth. Geomech. 38(4), 370-390.

Guo, N., Zhao, J., 2014. A coupled FEM/DEM approach for hierarchical multiscale modelling of granular media. Int. J. Numer. Meth. Eng. 99, 789-818.

Gutierrez, M., Ishihara, K., Towhata, I., 1991. Flow theory for sand during rotation of principal stress direction. Soils Found. 31 (4), 121-132.

Gutierrez, M., Ishihara, K., Towhata, I., 1993. Model for the deformation of sand during rotation of principal stress directions. Soils Found. 33 (3), 105-117.

Hashiguchi, K., Tsutsumi, S., 2003. Shear band formation analysis in soils by the subloading surface model with tangential stress rate effect. Int. J. Plasticity 19, 1651-1677.

Ishihara, K., Towhata, I., 1983. Sand response to cyclic rotation of principal stress directions as induced by wave loads. Soils Found. 23 (4), 11-26.

Lashkari, A., Latifi, M., 2008. A non-coaxial constitutive model for sand deformation under rotation of principal stress axes. Int. J. Numer. Anlyt. Meth. Geomech. 32, 1051-1086.

Li, X.S., 2013. Physical and mathematical bases of elastoplastic theories on saturated soils-in memory of professor HUANG Wenxi. Chinese J. Geotech. Eng. 35 (1), 1-33. (in Chinese)

Li, X.S., Dafalias, Y.F., 2004. A constitutive framework for anisotropic sand including non-proportional loading. Géotechnique 54 (1), 41-55.

Li, X.S., Dafalias, Y.F., 2012. Anisotropic critical state theory: the role of fabric. J. Eng. Mech. 138 (3), 263-275.

Li, X.S., Dafalias, Y.F. 2015. Dissipation consistent fabric tensor definition from DEM to continuum for granular media. J. Mech. Phys. Solids 78, 141-153.

Li, X., Yu, H.S., 2009. Influence of loading direction on the behaviour of anisotropic granular materials. Int. J. Eng. Sci. 47 (11-12), 1284-1296.

Li, X., Yu, H.S., 2010. Numerical investigation of granular material behaviour under rotational shear. Gétechnique 60 (5), 381-394.

Li, X., Yu, H., 2015. Particle-scale insight into deformation noncoaxiality of granular materials. Int. J. Geomech. 15 (4), 04014061.

Li, X.S., Wang, Y., 1998. Linear representation of steady-state line for sand. J. Geotech. Geoenvorn. Eng. 124 (12), 1215-1217.

Miura, K., Miura, S., Toki, S., 1986. Deformation behaviour of anisotropic dense sand under principal stress axes rotation. Soils Found. 26 (1), 36-52.

Nakata, Y., Hyodo, M., Murata, H., Yasufuku, N., 1998. Flow deformation of sands subjected to principal stress rotation. Soils Found. 38 (2), 115-128.

Nemat-Nasser, S., Zhang, J., 2002. Constitutive relations for cohesionless frictional granular materials. Int. J. Plasticity 18, 531-547.

Nicot, F., Darve, F., 2007. Basic features of plastic strains: from micro-mechanics to incrementally nonlinear model. Int. J. Plasticity 23, 1555-1588.

Oda, M., Konishi, J., 1974. Rotation of principal stresses in granular material during simple shear. Soils Found. 14, 39-53.

Papamichos, E., Vardoulakis, I., 1995. Shear band formation in sand according to non-coaxial plasticity model. Géotechnique 45 (4), 649-661.

Qian, J., Yang, J., Huang, M., 2008. Three-dimensional noncoaxial plasticity modeling of shear band formation in geomaterials. J. Eng. Mech. 134 (4), 322-329.

Richart, Jr F.E., Hall, J.R., Woods, R.D., 1970. Vibrations of soils and foundations. Englewood Cliffs, NJ: Prentice-Hall.

Rodriguez, N.M., Lade, P.V., 2014. Non-coaxiality of strain increment and stress directions in cross-anisotropic sand. Int. J. Solids Struct. 51 (5), 1103-1114.

Roscoe, K.H., 1970. The influence of strains in soil mechanics. The 10th Rankine Lecture, Géotechnique 20, 129-170.

Sloan, S.W., Abbo, A.J., Sheng, D., 2001. Refined explicit integration of elastoplastic models with automatic error control. Eng. Comput., 18 (1/2), 121-194.

Symes, M.J., Gens, A., Hight, D.W., 1984. Undrained anisotropy and principal stress direction rotation in saturated sand. Géotechnique 34 (1), l-27.

Symes, M.J., Gens, A., Hight, D.W., 1998. Drained principal stress rotation in saturated sand. Géotechnique 38 (1), 59-81.

Thorton, C., Zhang, L., 2006. A numerical examination of shear banding and simple shear non-coaxial flow rules. Philosophical Magazine 86, 21-22.

Tobita, Y., Yanagisawa, E., 1992. Modified stress tensor for anisotropic behaviour of granular materials. Soils Found 32 (1), 85-99.

Tong, Z., Zhang, J., Yu, Y., Zhang, G., 2010. Drained deformation behaviour of anisotropic sands during cyclic rotation of principal stress axes. J. Geotech. Geoenviron. Eng. 136 (11), 1509-1518.

Wan, R.G., Guo, P.J., 2004. Stress dilatancy and fabric dependencies on sand behavior. J. Eng. Mech. 130 (6), 635-645.

Wang, C.C., 1970. A new representation theorem for isotropic functions: An answer to Professor G. F. Smith's criticism of my papers on representations for isotropic functions. II. Vector-valued isotropic functions, symmetric tensor-valued isotropic functions, and skew-symmetric tensor-valued isotropic functions. Archive for Rational Mechanics and Analysis 36, 198-223.

Yang, D.S., 2013a. Microscopic study of granular material behaviours under general stress paths. PhD thesis, The University of Nottingham, UK.

Yang, L.T., 2013b. Experimental study of soil anisotropy using hollow cylinder testing. PhD thesis, The University of Nottingham, UK.

Yang, Y., Fei, W., Yu, H.S., Ooi, J., Rotter, M., 215. Experimental study of anisotropy and non-coaxiality of granular solids. Granular Matter 17, 189-196.

Yang, Z.X., Li, X.S., Yang, J., 2007. Undrained anisotropy and rotational shear in granular soil. Géotechnique 57 (4), 371-384.

Yoshimine, M., Ishihara, K., Vargas, W., 1998. Effects of principal stress direction and intermediate principal stress on undrained shear behaviour of sand. Soils Found. 38 (3), 179-188.

Yu, H.S., Yuan, X., 2006. On a class of non-coaxial plasticity models for granular soils. Proceedings of Royal Society London Series A 426 (2067), 725-748.

Yu, H.S., 2008. Non-Coaxial theories of plasticity for granular materials. Proceedings of the 12th International Conference of International Association for Computer Methods and Advances in Geomechanics (IACMAG), Goa, India, 361-378.

Zhao, J., Gao, Z., 2016. Unified anisotropic elasto-plastic model for sand. J. Eng. Mech. 142 (1), 04015056.

Zhao, J., Guo, N., 2015. The interplay between anisotropy and strain localisation in granular soils: a multiscale insight. Géotechnique 65 (8), 642-656.

Zhao, J., Sheng, D., Rouainia, M., Sloan, S.W., 2005. Explicit stress integration of complex soil models. Int. J. Numer. Anal. Meth. Geomech., 29 (12), 1209-1229.